Journal of Sound and Vibration (1998) **209**(5), 821–843

EFFECTS OF NON-HOMOGENEITIES ON THE EIGENMODES OF ACOUSTIC PRESSURE IN COMBUSTION CHAMBERS

J. S. KIM† AND F. A. WILLIAMS

Center for Energy and Combustion Research, University of California, San Diego La Jolla, CA 92093-0411, *U.S.A.*

(*Received* 7 *June* 1996, *and in final form* 9 *September* 1997)

Modifications to acoustic eigenmodes in combustion chambers such as those of liquid propellant rocket engines, produced by spatial variations of density and sound speed that arise mainly through progress of combustion processes, are analyzed by using a variational method. The variational principle shows that the eigenvalue is the ratio of a weighted acoustic kinetic energy to a weighted acoustic potential energy, and the eigenfunction is the minimizing function of this ratio. A sample calculation is made for the case in which variations of the properties occur dominantly in the longitudinal direction, with lower temperatures and higher densities prevailing near the injector. The results of the calculation exhibit two major characteristics: the longitudinal density variation aids transfer of acoustic kinetic energy from a lower mode to the adjacent higher mode, so that the pure transverse modes have substantially larger reductions (sometimes exceeding 50%) of their eigenvalues than the combined modes; and variations of the acoustic pressure gradients are found to be larger in high-density regions, so that the acoustic pressure amplitude for purely tangential modes is found to be much higher near the injector than near the nozzle. The higher head acoustic pressure may contribute to the greater sensitivity of acoustic instability to characteristics of the flames near the injectors, as commonly found in engine tests. The improved acoustic eigensolutions can also be helpful in sizing damping devices, such as baffles or acoustic liners.

1. INTRODUCTION

Acoustic instabilities in liquid-propellant rock engines are phenomena in which oscillations of the chamber pressure at well-defined frequencies and mode shapes that correspond to the acoustic modes of the cavity are amplified mainly through interactions with combustion [1–3]. Acoustic waves in these and other combustion devices possess various modes of oscillation that are usually analyzed under the assumption that the mean field is uniform and stationary, so that the acoustic modes are described by homogeneous Helmholtz equations. In most of the linear and non-linear analyses developed to date [4–7], acoustic pressure is expressed as a sum of classical Helmholtz eigenmodes with non-steady amplitudes. However, this assumption must have inaccuracies because of the presence of combustion, which can give rise to order-of-magnitude variations of temperature in the combustion chamber. In general, acoustic pressure tends to oscillate faster in a

† Present Address: Environment Research Center, Korea Institute of Science and Technology, PO Box 131, Cheongryang, Seoul, 130–650 Korea.

0022–460X/98/050821 + 23 $25.00/0/sv971324

higher-temperature medium because of the increased sound speed, and it is of interest to find what the oscillation frequencies will be and what the acoustic pressure distributions will look like when an acoustic medium is strongly non-uniform in temperature and in other thermodynamic variables. This paper presents a method of analysis to address these questions and attempts to draw general conclusion concerning what modifications of acoustic characteristics should be expected in non-uniform media.

A few investigations have been reported previously concerning the influences of non-uniformities on acoustic modes in chambers. Most of these have been restricted to one-dimensional mean-field variations that occur only in the longitudinal direction [8–15]. When the variations occur only in one dimension, it is straightforward to transform the variable in that direction to an inversely mass weighted co-ordinate, in such a way that a Helmholtz equation with variable sound speed is retrieved in the transformed variables. More conventional analyses then apply in the transformed co-ordinates, although most of the studies cited above do not take advantage of this simplification. Such a simple transformation of variables cannot be employd for general, three-dimensional variations of mean properties. In the present work, a variational approach [16], that is capable of accounting for these three-dimensional mean-field distributions and not previously applied to combustion instability is introduced. Nevertheless, for the purpose of drawing readily comprehensible qualitative conclusions form the results, attention will be focused on influences of purely longitudinal mean-property variations. For acoustic modes having high-frequency axial components, a WKB approach yields such qualitative information [9], but attention here is focused instead on situations involving low-frequency longitudinal mode components, the fundamental or first or second harmonic, which are more commonly encountered in combustion instability.

With three-dimensional variations of mean-field properties, numerical methods, such as finite element methods [17], can be invoked for finding the acoustic modes. Although these methods can provide accurate answers for specific chambers when the mean fields are known, they do not lend themselves easily to drawing general conclusions about qualitative behaviors. There is empirical information on qualitative differences from uniform-property behavior. For example, there are indications that observed frequencies are often lower than calculated from assumptions of uniform chamber properties [11, 18]. A possible reason for this will be obtained in the present study, and a method for estimating the magnitude of the effect will be given.

The typical acoustic instability involves two-time behavior, in which combustion produces an amplification time that is long compared with the acoustic time. Certain acoustic modes then grow slowly in amplitude, in a manner that can be described by a linear analysis. For calculating this linear amplification, it is important to have accurate representations of the acoustic mode shapes and their frequencies. This information is also needed for non-linear analyses that address bifurcation phenomena [19, 20]. Although there are resonance-tube applications for pulse combustors in which influences of combustion and non-uniformities on the acoustic modes can be negligible [20], in liquid-propellant rocket chambers these influences can often be important. An objective of the present study is to provide a method for obtaining the leading-order acoustic behavior, the acoustic frequencies and mode shapes, needed for pursuit of such non-linear analyses for liquid-propellant rockets, which had to be simply postulated in our recent investigation [21] of the subject. In addition, non-Helmholtz eigenmodes may lead to a change in the orthogonality, giving rise to additional terms in describing non-linear analyses that result from interaction of acoustics with non-uniform steady mean fields.

2. FORMULATION

2.1. CONSERVATION EQUATIONS

A detailed derivation of the conservation equations, generalizing simpler results [22] and applicable to multiphase viscous reacting flows, is given by Kim [23]. In the notation adopted here, all variables carrying a "tilde" are dimensional. Non-dimensionalization of the variables will be introduced in the next subsection. The conservation equations for pressure and velocity, that can include both acoustic and entropy waves, can be written as

$$\tilde{\kappa}_f \frac{D\tilde{p}}{D\tilde{t}} + \tilde{\nabla} \cdot \tilde{\mathbf{u}} = \tilde{Q}, \qquad \tilde{\rho} \frac{D\tilde{\mathbf{u}}}{D\tilde{t}} + \tilde{\nabla}\tilde{p} = \tilde{\mathbf{F}}, \tag{1}$$

where the overall frozen adiabatic compressibility $\tilde{\kappa}_f$ is

$$\tilde{\kappa}_f \equiv \frac{1}{\tilde{\rho}} \left(\frac{\partial \tilde{\rho}}{\partial \tilde{p}} \right)_{\tilde{s}, Y_{ji}} = \frac{1}{\tilde{\rho}\tilde{a}_f^2}. \tag{2}$$

Here the material derivative is defined as $D/D\tilde{t} \equiv \partial/\partial\tilde{t} + \tilde{\mathbf{u}} \cdot \tilde{\nabla}$.

The source terms $\tilde{Q}$ and $\tilde{\mathbf{F}}$ arise from a number of effects. The energy source term $\tilde{Q}$, denoting the rate of heat transfer per unit mass, includes various contributions from molecular transport, contributions from relative velocities, contributions from phase change and contributions from exothermic chemical reaction. The exothermic chemical reaction is often the most important among these contributions. In a similar manner, $\tilde{\mathbf{F}}$ represents the momentum transfer resulting from viscous stresses and from the relative velocities of different phases. Both $\tilde{Q}$ and $\tilde{\mathbf{F}}$ thus contain some higher-derivative terms, included here with sources. One proper way to evaluate $\tilde{\kappa}_f$ in multiphase flows is given in Appendix A.

2.2. NON-DIMENSIONALIZATION AND SCALINGS

It is important to recognize that variations of the mean field and of the acoustic field scale differently, since the mean field is measured by a characteristic flow velocity, whereas the acoustic field refers to a characteristic sound speed. Attention is focused on the condition of a small Mach number, thereby providing a scaling which ultimately yields a substantially simplified wave equation.

To proceed with non-dimensionalization, reference values for the velocity and density need to be selected. In non-uniform acoustic media, choice of the reference values is not unique. However, any unambiguous choice with a proper order of magnitude will yield the same result. First, the reference density and adiabatic compressibility are obtained by volumetric averages in the steady pre-instability state,

$$\tilde{\rho}_0 = \int_{\mathscr{V}} \frac{\tilde{\rho}\, \mathrm{d}\tilde{\mathbf{x}}}{\tilde{V}}, \qquad \tilde{\kappa}_0 = \int_{\mathscr{V}} \frac{\tilde{\kappa}_f\, \mathrm{d}\tilde{\mathbf{x}}}{\tilde{V}}. \tag{3}$$

From $\tilde{\rho}_0$ and $\tilde{\kappa}_0$, the characteristic velocity scales for the acoustic and mean fields are found to be

$$\tilde{a}_0 = 1/(\tilde{\kappa}_0\, \tilde{\rho}_0)^{1/2}, \qquad \tilde{u}_0 = \tilde{m}/\tilde{\rho}_0, \tag{4}$$

where the area-averaged axial mass flux $\tilde{m}$ is assumed to be constant in the undisturbed state, as it is during steady motor operation. Then the Mach number M is defined as

$$M \equiv \tilde{u}_0/\tilde{a}_0 = \tilde{m}/\tilde{\rho}_0\, \tilde{a}_0 = \tilde{m}(\tilde{\kappa}_0/\tilde{\rho}_0)^{1/2}, \tag{5}$$

which is also a ratio of a characteristic acoustic time to a characteristic flow time. In addition, the characteristic length scale is the rocket chamber length $\tilde{L}$.

We define the non-dimensional space and time co-ordinates

$$\mathbf{x} \equiv \frac{\tilde{\mathbf{x}}}{\tilde{L}}, \qquad t \equiv \frac{\tilde{a}_0\, t}{\tilde{L}}. \tag{6}$$

The non-dimensional dependent variables are

$$p \equiv \frac{\tilde{p}}{\tilde{\rho}_0\, \tilde{a}_0^2}, \qquad \mathbf{u} = \frac{\tilde{\mathbf{u}}}{\tilde{a}_0}, \qquad \rho \equiv \frac{\tilde{\rho}}{\tilde{\rho}_0}, \qquad \kappa = \frac{\tilde{\kappa}_f}{\tilde{\kappa}_0}. \tag{7}$$

On the other hand, momentum transfer of the mean field occurs in a characteristic flow time. In the mean field, appropriate non-dimensionalizations for the velocity and for the pressure variation are

$$p_s = \frac{\tilde{p}_s}{\tilde{\rho}_0\, \tilde{u}_0^2} = M^{-2}\, \frac{\tilde{p}_s}{\tilde{\rho}_0\, \tilde{a}_0^2}, \qquad \mathbf{u}_s = \frac{\tilde{\mathbf{u}}_s}{\tilde{u}_0} = M^{-1}\, \frac{\tilde{\mathbf{u}}_s}{\tilde{a}_0}, \tag{8}$$

where the subscript s denotes the steady field variables. In addition, with the non-dimensionalization of equation (7), there exists a constant mean non-dimensional static pressure p_0 of order unity. Finally, the source term $\tilde{Q}$ and $\tilde{\mathbf{F}}$ in equation (1) are scaled as

$$Q \equiv \frac{\tilde{L}\tilde{Q}}{\tilde{a}_0}, \qquad \mathbf{F} \equiv \frac{\tilde{L}\tilde{\mathbf{F}}}{\tilde{a}_0^2}, \tag{9}$$

while the mean source terms are alternatively scaled as

$$Q_s = \frac{\tilde{L}\tilde{Q}_s}{\tilde{u}_0} = M^{-1}\, \frac{\tilde{L}\tilde{Q}_s}{\tilde{a}_0}, \qquad \mathbf{F}_s = \frac{\tilde{L}\tilde{\mathbf{F}}_s}{\tilde{u}_0^2} = M^{-2}\, \frac{\tilde{L}\tilde{\mathbf{F}}_s}{\tilde{a}_0^2}. \tag{10}$$

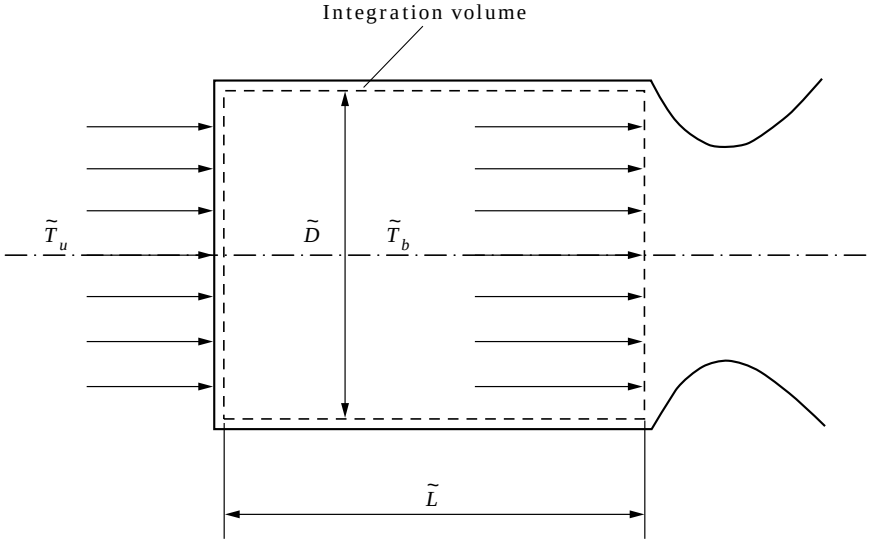

Figure 1. Schematic diagram of liquid propellant rocket engine and integration domain.

2.3. DERIVATION OF THE GENERALIZED HELMHOLTZ EQUATION

To begin the analysis, it is necessary to decompose the dependent variables into sums of the mean and acoustic components. The acoustic field can be sought as an expansion in powers of a small parameter ε that measures the amplitude of the acoustic pressure relative to the mean static pressure. According to the scalings described above, we seek a solution in the form

$$\begin{aligned} p &= p_0 + M^2 p_s + \varepsilon \wp_1 + \varepsilon^2 \wp_2 + \cdots, \\ \mathbf{u} &= M\mathbf{u}_s + \varepsilon \mathbf{v}_1 + \varepsilon^2 \mathbf{v}_2 + \cdots, \\ \rho &= \rho_s + \varepsilon \varrho_1 + \varepsilon \varrho_2 + \cdots, \\ \kappa &= \kappa_2 + \varepsilon \kappa_1 + \varepsilon^2 \kappa_2 + \cdots, \\ Q &= M(Q_s + \varepsilon q_1 + \varepsilon^2 q_2 + \cdots), \\ \mathbf{F} &= M^2(\mathbf{F}_s + \varepsilon \mathbf{f}_1 + \varepsilon^2 \mathbf{f}_2 + \cdots). \end{aligned} \tag{11}$$

The additional terms involve various higher power of M and ε.

Although not pursued in the present analysis, it is worthy of note that a proper scaling of ε with the Mach number M enables us to extend the present analysis to non-linear bifurcation analysis. The scaling, which was already recognized by Margolis [20] for the resonance-tube problem, is also applicable to combustion instabilities of rocket engines. In his work, the small parameter ε was scaled as $\varepsilon = \sqrt{M}$ and the slow time $\hat{t} = \varepsilon^2 t = Mt$.

Substituting equation (11) into equation (1) and collecting the terms of order ε, we obtain linear homogeneous equations for the leading-order acoustic pressure and velocity fields, $\wp_1$ and $\mathbf{v}_1$, in the form

$$\rho_s \frac{\partial \mathbf{v}_1}{\partial t} + \nabla \wp_1 = 0, \qquad \kappa_s \frac{\partial \wp_1}{\partial t} + \nabla \cdot \mathbf{v}_1 = 0. \tag{12}$$

These equations describe the acoustic profiles of pressure and velocity with non-uniform distributions of the density and adiabatic compressibility.

At the leading order, the boundary condition for equation (12) is taken to be

$$\mathbf{n} \cdot \nabla \wp_1 = 0. \tag{13}$$

In principle, this homogeneous Neumann condition is applicable only to solid walls through which no heat and mass transfer occurs, while the boundaries at the injector and at the entrance to the nozzle usually have finite pressure gradients. However, the pressure gradients at these boundaries generally are sufficiently small so that equation (13) is the best choice for defining the first approximation to the acoustic modes.

Since a differential equation with a single dependent variable is often easier to handle than a pair of equations, we eliminate $\mathbf{v}_1$ from equation (12). The acoustic equation is thereby found to be

$$\nabla \cdot \left(\frac{\nabla \wp_1}{\rho_s} \right) - \kappa_s \frac{\partial^2 \wp_1}{\partial t^2} = 0. \tag{14}$$

Since each eigenmode of the acoustic pressure oscillates harmonically in time, equation (14) can be further simplified by introducing the complex representation of the acoustic pressure

$$\wp_1 = Re\ \{\psi \exp(\mathrm{i}\lambda t)\}, \tag{15}$$

where a non-dimensional frequency λ is to be determined as a part of the solution. The dimensional acoustic frequency $\tilde{\omega}$ is directly related to λ by

$$\tilde{\omega} = \frac{\lambda}{\tilde{L}} \sqrt{\frac{1}{\tilde{\kappa}_0 \, \tilde{\rho}_0}}. \tag{16}$$

The corresponding acoustic velocity can be found from the first expression in equation (12) to be

$$\mathbf{v}_1 = \frac{Re \, \{\mathrm{i} \nabla \psi \, \exp(\mathrm{i}\lambda t)\}}{\lambda \rho_s}. \tag{17}$$

Upon substitution of equation (15) into equation (14), the governing equation for ψ is found to be

$$\nabla \cdot \left(\frac{\nabla \psi}{\rho_s} \right) + \lambda^2 \kappa_s \, \psi = 0, \qquad \text{with} \quad \mathbf{n} \cdot \nabla \psi = 0 \quad \text{at boundaries.} \tag{18}$$

If ρ_s and κ_s are constant thorughout the rocket chamber, then equation (18) reduces to the ordinary Helmholtz equation with wave number $\tilde{k} = \lambda / \tilde{L}$. Equation (18) is available from a number of sources [24, 25].

3. APPROXIMATION METHOD

3.1. VARIATIONAL PRINCIPLE

For notational brevity, equation (18) is symbolically expressed as

$$\mathscr{L} \psi = \sigma \mathscr{M} \psi, \tag{19}$$

where a differential operator $\mathscr{L}$, a weighting function $\mathscr{M}$ and an eigenvalue σ are defined as

$$\mathscr{L} \equiv -\nabla \cdot (\rho_s^{-1} \nabla), \qquad \mathscr{M} \equiv \kappa_s, \qquad \sigma \equiv \lambda^2. \tag{20}$$

In what follows, an approximation method based on a variational principle will be discussed; details can be found in Meirovitch [16], Morse and Feshbach [26], and Gelfand and Fomin [27].

As a first step, the inner product is defined by

$$\langle f, g \rangle \equiv \int_{\mathscr{V}} fg \, \mathrm{d}\mathbf{x}. \tag{21}$$

It can be easily shown through integration by parts that

$$\langle \varphi, \mathscr{L} \psi \rangle = -\int_{\mathscr{V}} \varphi \nabla \cdot (\rho_s^{-1} \nabla \psi) \, \mathrm{d}\mathbf{x} = \int_{\mathscr{V}} \rho_s^{-1} \nabla \varphi \cdot \nabla \psi \, \mathrm{d}\mathbf{x}, \tag{22}$$

which leads to $\langle \varphi, \mathscr{L}\psi \rangle = \langle \mathscr{L}\varphi, \psi \rangle$. This result states that the problem is *self-adjoint*. For self-adjoint problems, the eigenvalues satisfy the relation

$$\sigma = \frac{\langle \psi, \mathscr{L}\psi \rangle}{\langle \psi, \mathscr{M}\psi \rangle} = \frac{\int_{\mathscr{V}} \rho_s^{-1} \nabla\psi \cdot \nabla\psi \, \mathrm{d}\mathbf{x}}{\int_{\mathscr{V}} \kappa_s \psi^2 \, \mathrm{d}\mathbf{x}}, \tag{23}$$

and the corresponding first-order variational principle assumes the form

$$\delta[\sigma] = \delta\left[\frac{\langle \psi, \mathscr{L}\psi \rangle}{\langle \psi, \mathscr{M}\psi \rangle}\right] = 0, \tag{24}$$

where $\delta[]$ denotes the variational operation for ψ. The eigenfunctions ψ_i and their corresponding eigenvalues σ_i can be obtained approximately from equations (23) and (24).

It is useful to recall several important properties of self-adjoint systems. First of all, the eigenfunctions are orthogonal with respect to their weighting function, i.e.,

$$\langle \psi_i, \mathscr{M}\psi_j \rangle = \int_{\mathscr{V}} \mathscr{M}\psi_i \psi_j \, \mathrm{d}\mathbf{x} = \delta_{ij}, \qquad i, j = 1, 2, 3, \ldots, \tag{25}$$

where ψ_i's are normalized in such a way that $\langle \psi_i, \mathscr{M}\psi_i \rangle = 1$. In addition, the operator $\mathscr{L}$ is *positive semi-definite* because $\langle \varphi, \mathscr{L}\varphi \rangle \geqslant 0$ for any φ, which can be easily seen from equation (22). From equation (23), all eigenvalues are then real and non-negative. The zero eigenvalue corresponds to the equality in the positive semi-definiteness. The corresponding eigenfunction is $\psi = (\int_{\mathscr{V}} \kappa_s \, \mathrm{d}\mathbf{x})^{1/2}$ and represents bulk pressure oscillations in the chamber with an infinitely long period. We exclude this trivial case and consider $\mathscr{L}$ to be positive definite. Whenever the operators $\mathscr{L}$ and $\mathscr{M}$ are self-adjoint and positive-definite,

$$\delta^2\left[\frac{\langle \psi, \mathscr{L}\psi \rangle}{\langle \psi, \mathscr{M}\psi \rangle}\right] = \frac{2\langle \delta[\psi], (\mathscr{L} - \sigma\mathscr{M})\delta[\psi] \rangle}{\langle \psi, \mathscr{M}\psi \rangle} > 0, \tag{26}$$

that is, the second variation is positive-definite too [27]. The eigenvalue σ_i is, therefore, a local minimum for the eigenfunction ψ_i with respect to the variation of ψ_i.

3.2. DISCRETIZATION

Solving the eigenvalue problem in equation (19) directly in closed form is usually not feasible, and the main interest lies in an approximate solution. The variational approach then becomes particularly attractive because a solution can be constructed from a space of admissible functions. Advantages arise from the fact that admissible functions need only satisfy the geometric boundary condition in equation (18) and be twice differentiable, and that such admissible functions are plentiful.

The *Rayleigh quotient* is defined as

$$R(\varphi) = \frac{\langle \varphi, \mathscr{L}\varphi \rangle}{\langle \varphi, \mathscr{M}\varphi \rangle}, \tag{27}$$

where φ is a trial function from the space of admissible functions. If the trial function is an eigenfunction, its first variation vanishes and the Rayleigh quotient becomes the corresponding eigenvalue. For practical reasons, we cannot consider the entire space of

eigenfunctions, but only a finite-dimensional subspace, where the subspace is spanned by the n linearly independent admissible functions, $\phi_1, \phi_2, \ldots, \phi_n$, from a complete set. For algebraic convenience, the admissible functions can be normalized such that $\langle \phi_i, \phi_i \rangle = 1$. Any element $\varphi^{(n)}$ in an n-dimensional subspace can be expanded in the finite series

$$\varphi^{(n)} = \sum_{i=1}^{n} c_i^{(n)} \phi_i, \tag{28}$$

where $c_1, c_2, \ldots, c_n$ are coefficients to be determined. For a given set of ϕ_i's, the Rayleigh quotient is now expressed as a function of c_i's. Then the first-order variational principle in equation (24) is effectively replaced by the *stationary condition*

$$\frac{\partial R}{\partial c_i} = 0, \qquad i = 1, 2, \ldots, n, \tag{29}$$

which ultimately determines the c_i's. The $\varphi^{(n)}$ satisfying the stationarity condition is an approximation to the exact solution.

Substituting the linearly expanded trial functions in equation (28) into equation (27), we can write the Rayleigh quotient in the discretized form

$$R = \frac{\sum_{i,j=1}^{n} c_i L_{ij} c_j}{\sum_{i,j=1}^{n} c_i M_{ij} c_j}, \tag{30}$$

where the known constant matrices L_{ij} and M_{ij} are

$$L_{ij} = \langle \phi_i, \mathscr{L}\phi_j \rangle = \int_{\mathscr{V}} \rho_s^{-1} \nabla\phi_i \cdot \nabla\phi_j \, \mathrm{d}\mathbf{x}, \qquad M_{ij} = \langle \phi_i, \mathscr{M}\phi_j \rangle = \int_{\mathscr{V}} \kappa_s \phi_i \phi_j \, \mathrm{d}\mathbf{x}. \tag{31}$$

Then it is not difficult to show that satisfaction of the stationarity conditions in equation (29) is equivalent to solution of the linear algebraic eigenvalue problem

$$L_{ij} c_i^{(n)} = \sigma^{(n)} M_{ij} c_i^{(n)}, \tag{32}$$

where $\sigma^{(n)}$ is the stationary value of the Rayleigh quotient in the n-dimensional subspace. The solution of the eigenvalue problem in equation (32) consists of n pairs of the approximate eigenvalues $\sigma_r^{(n)}$ and the associated unit eigenvectors $c_{i,r}^{(n)}$ $(r = 1, 2, \ldots, n)$ that are normalized by the orthonormality $\Sigma_{i,j=1}^{i} c_{i,r}^{(n)} M_{ij} c_{j,s}^{(n)} = \delta_{rs}$. Conventionally the subscript index r denoting the eigensolutions is ordered from the solution with the smallest eigenvalue. As n increases, the approximated eigensolutions approach the exact eigensolutions.

Although convergence is guaranteed if the admissible functions ϕ_i are selected from a complete set, the rate of convergence depends on the nature of the admissible functions. Hence, the choice of the admissible functions can be very important. The best choice of the admissible functions for equation (18) is obviously a set of Helmholtz eigenfunctions satisfying the Neumann boundary condition. It is also relevant to note that convergence of the eigenvalues is much faster than that of the eigenfunctions. Because the first variation vanishes for the exact solutions, the eigenvalues have only second-order error for first-order error of the eigenfunctions. In addition, the approximated eigenvalues converge to the actual values from above, since the second variation is positive-definite. These

properties of the eigenvalue's convergence enable us to adopt a systematic way of monitoring the convergence. The number of admissible functions, n, can be gradually increased from a small number to a certain number satisfying whatever convergence requirement is imposed. More accurate eigenvalues can subsequently be obtained by using the Richardson or Padé extrapolation [28].

4. A SIMPLIFIED MODEL PROBLEM

4.1. TRANSVERSELY UNIFORM ACOUSTIC MEDIA

In many rocket engines, transverse variations of the steady profiles of the temperatures and other properties are small compared with those in the longitudinal direction, and it becomes reasonable to introduce the approximation that variations of the density and adiabatic compressibility occur only longitudinally. Combined with this assumption, the additional fact that Helmholtz eigenfunctions are separable in the transverse and longitudinal further simplifies the calculation procedure.

As a first step in computing eigensolutions for axisymmetric chambers, we choose $m \times n$ addmissible functions from a set of Helmholtz eigenfunctions, where m is the number of the chosen transverse modes, and n is the number of the longitudinal modes. The admissible functions can then be arranged in such a way that

$$\phi_i = \Theta_p\,(r, \theta)\Lambda_q\,(z), \qquad i = np + q, \qquad p = 1, 2, \ldots, m, \qquad q = 1, 2, \ldots, n, \quad (33)$$

where Θ_p is the pth normalized Helmholtz transverse mode, and Λ_q the qth normalized longitudinal mode. By substituting equation (33) into equation (31), a linear algebraic eigenvalue problem can be constructed in the form of equation (32). For two arbitrarily chosen admissible functions

$$\phi_i = \Theta_p\,\Lambda_q, \qquad \phi_j = \Theta_r\,\Lambda_s, \qquad i = np + q, \qquad j = nr + s,$$

the matrices L_{ij} and M_{ij} become

$$L_{ij} = \int_{\mathscr{V}} \rho_s^{-1}\,\nabla\phi_i \cdot \nabla\phi_j\,\mathrm{d}\mathbf{x} = \delta_{pr}\left[k_p^2 \int_0^1 \frac{\Lambda_q\,\Lambda_s\,\mathrm{d}z}{\rho_s} + \int_0^1 \frac{1}{\rho_s}\frac{\mathrm{d}\Lambda_q}{\mathrm{d}z}\frac{\mathrm{d}\Lambda_s}{\mathrm{d}z}\,\mathrm{d}z\right],$$

$$M_{ij} = \int_{\mathscr{V}} \kappa_s\,\phi_i\,\phi_j\,\mathrm{d}\mathbf{x} = \delta_{pr}\int_0^1 \kappa_s\,\Lambda_q\,\Lambda_s\,\mathrm{d}z, \quad (34)$$

where k_p is the non-dimensional wave number of Θ_p, and use has been made of

$$-\int_0^R \int_0^{2\pi} \nabla\Theta_p \cdot \nabla\Theta_r\,r\,\mathrm{d}r\,\mathrm{d}\theta = k_p^2\,\delta_{pr}, \qquad \int_0^R \int_0^{2\pi} \Theta_p\,\Theta_r\,r\,\mathrm{d}r\,\mathrm{d}\theta = \delta_{pr}.$$

It is seen from equation (34) that the matrices L_{ij} and M_{ij} are block-diagonal, where each non-zero block corresponds to a different transverse mode. Since the linear eigenvalue problem is meaningful only if $p = r$, each block forms a separate eigenvalue problem. In other words, for a given transverse mode, all components of the eigenvector corresponding to any other transverse mode vanish. The resulting transverse eigenmode shape thus remains the same as the Helmholtz eigenmode. The problem now reduces to that of determining only the longitudinal modes for a given transverse mode.

4.2. A SAMPLE CALCULATION

To generate illustrative results, the acoustic medium is assumed to be a mixture of gas and liquid phases far from critical conditions, so that the gas phase is a mixture of ideal gases. The aspect ratio of the combustion chamber is taken to be unity, $\tilde{D}/\tilde{L} = 1$, where $\tilde{D}$ is the chamber diameter. Attention is focused on the first tangential mode, usually the most common acoustic mode observed in liquid-propellant rocket engines, for example. Then the functional form of the transverse mode is

$$\Theta(r, \theta) = \frac{J_1(k_{11} r) \sin \theta}{\left\{\pi \int_0^{1/2} J_1^2(k_{11} r)\, \mathrm{d}r\right\}^{1/2}}, \tag{35}$$

where k_{11} is the non-dimensional wave number for the first tangential mode; $k_{11} = 3{\cdot}6826$ for $\tilde{D}/\tilde{L} = 1$. A set of admissible functions are

$$\phi_i = \begin{cases} \Theta & \text{if } i = 1, \\ \Theta\sqrt{2} \cos[(i-1)\pi z] & \text{if } i \neq 1. \end{cases} \tag{36}$$

The density profile is assumed to be

$$\frac{1}{\rho_s} = 1 - \tfrac{3}{4} \cos \pi z, \tag{37}$$

for which the density at the exit is only one-seventh of that at the injector, which can be reasonable for some liquid-propellant rockets. Such a large decrease in density can be caused by the decrease in mass fraction of the liquid phase and by the increase in temperature during combustion. The density variation is approximated in the form of equation (37) because the dominant Fourier component of the density variation is the first harmonic. As discussed in Appendix A, the adiabatic compressibility κ_f is proportional to volume fraction of the gas phase and inversely proportional to the chamber pressure. Since the volume fraction of the liquid phase is always small and the variation of the mean chamber pressure is of order M^2, the adiabatic compressibility is taken to be $\kappa_f = 1$ in this illustrative example.

From the above assumptions, the matrices M_{ij} and L_{ij} are found to be

$$M_{ij} = \delta_{ij}, \qquad L_{ij} = \begin{cases} k_{11}^2 + (i-1)^2\pi^2 & \text{if } i = j, \\ -\dfrac{3\sqrt{2}}{8} k_{11}^2 & \text{if } ij = 2, \\ -\tfrac{3}{8}[k_{11}^2 + (i-1)(j-1)\pi^2] & \text{if } |i-j| = 1 \text{ and } ij \neq 2 \\ 0 & \text{otherwise.} \end{cases} \tag{38}$$

As mentioned in the introduction, transformation into an inversely mass-weighted co-ordinate may be considered in order to eliminate the density variation in the modified Laplacian operator. Such transformation will result in a simpler formulation if κ_f and ρ_s are not constant in the flow field. Then the resulting modified Helmholtz equation involves only the variation of the κ_f/ρ_s term. If the κ_f/ρ_s term is constant throughout the flow field, the modified Helmholtz equation is further simplified to recover the original Helmholtz equation in the transformed co-ordinate. However, the present case does not fall into either

TABLE 1

Comparison of the eigenvalues with and without the variable density profile. In each box, the smaller number on the top is the computed eigenvalue with the variable density profile, while the larger number at the bottom is that corresponding to the Helmholtz eigenvalue (uniform chamber)

	1st Tangential 1T $J_1(k_{11}\,r)\sin\theta$	2nd Tangential 2T $J_2(k_{21}\,r)\sin 2\theta$	1st Radial 1R $J_0(k_{01}\,r)$	3rd Tangential 3T $J_3(k_{31}\,r)\sin 3\theta$
Pure transverse	8·566	17·267	24·219	27·933
0L	13·562	37·315	58·728	70·600
1st Longitudinal	21·624	43·856	58·228	65·187
1L	23·431	47·185	68·597	80·470
2nd Longitudinal	41·288	66·723	90·948	102·99
2L	53·040	76·793	98·206	110·08
3rd Longitudinal	77·511	98·692	120·23	133·46
3L	102·39	126·14	147·55	159·43

of the two cases, and does not reduce to any simpler formulation by transforming into an inversely mass-weighted co-ordinate.

The method is also capable of calculating the acoustic eigenmodes in three dimensions and, as indicated in section 3, the convergence is guaranteed if the admissible functions are chosen from a complete set. For rocket-engine applications, it will be the best to choose the admissible functions from a complete set of spherical harmonic functions.

4.3. RESULTS OF SAMPLE CALCULATION AND THEIR EXPLANATION

The results of the calculation are shown in the first column of Table 1 for the eigenvalues of the first four longitudinal eigenmodes and in Figures 2 through 4 for the longitudinal variations of their eigenfunctions. Convergence of the eigenvalues with four-digit accuracy is achieved by employing less than 12 trial functions. For the pure first tangential mode, denoted by 1T-0L, the calculated eigenvalue is about 2/3 of the corresponding Helmholtz eigenvalue. If the acoustic frequency is estimated by equations (16) and (20), the resulting frequency will be about 20% smaller than its Helmholtz counterpart (uniform chamber), comparable to the reduction observed in some measurements [18]. For the combined modes of the first tangential, respectively denoted by 1T-1L, 1T-2L and 1T-3L, the resulting eigenvalues are smaller than the corresponding Helmholtz eigenvalues by 10–25%. Variations of the acoustic eigenfunctions $\varphi_i^{(n)}$ with different numbers of trial functions are shown in Figures 2 and 3 for 1T-0L and 1T-1L, respectively. Convergence of the functional shapes is achieved by less than 10 trial functions, although the degree of convergence is not as good as that for the eigenvalues. However, the most pronounced feature of the resulting acoustic eigenfunctions is that the gradients of the acoustic pressure amplitudes are much steeper near the chamber entrance than near the exit. In other words, the variations take place dominantly in the high-density region. The same characteristics are found in Figure 4 for the higher acoustic modes.

To explain the results obtained from the sample calculation. it is convenient to consider the total acoustic energy e, which is defined by

$$e = \tfrac{1}{2}\int_{\mathscr{V}} \kappa_s\, \wp_1^2\, \mathrm{d}\mathbf{x} + \tfrac{1}{2}\int_{\mathscr{V}} \rho_s\, \mathbf{v}_1 \cdot \mathbf{v}_1\, \mathrm{d}\mathbf{x}, \tag{39}$$

where the first and second parts of the right-hand side represent the potential and kinetic acoustic energy, respectively. Taking only the real parts of the acoustic pressure and velocity in equations (15) and (17) and substituting into equation (39), the total acoustic energy is expressed, in terms of ψ, by

$$e = \tfrac{1}{2}\int_{\mathscr{V}} \kappa_s \psi^2 \, d\mathbf{x} + \frac{\sin^2(\lambda t)}{2}\left[\int_{\mathscr{V}} \frac{\nabla\psi \cdot \nabla\psi}{\lambda^2 \rho_s} \, d\mathbf{x} - \int_{\mathscr{V}} \kappa_s \psi^2 \, d\mathbf{x}\right]. \tag{40}$$

Because there is no acoustic energy source or sink in the leading-order acoustic equation, the total acoustic energy must be constant in time. This can be satisfied only if the term involving $\sin^2(\lambda t)$ in the above equation vanishes. The resulting equation then turns out to be identical to equation (23) which expresses the eigenvalue σ as a ratio of volumetric integrals. The fact that equation (23) states conservation of the total acoustic energy is rather obvious because equation (23) is obtained by an energy integral. Of course, amplification or attenuation mechanisms will cause the acoustic energy to vary [22].

If an acoustic medium is uniform, the Helmholtz eigenfunctions are the minimizing functions of the functional given in equation (23). As the acoustic medium is perturbed from a uniform state, the acoustic pressure amplitude must adjust its functional form in order to minimize the functional in equation (23). In this sample calculation, the non-dimensional adiabatic compressibility κ_s is constant, so that the minimization process occurs mainly in the numerator. This can be achieved by distributing more evenly the

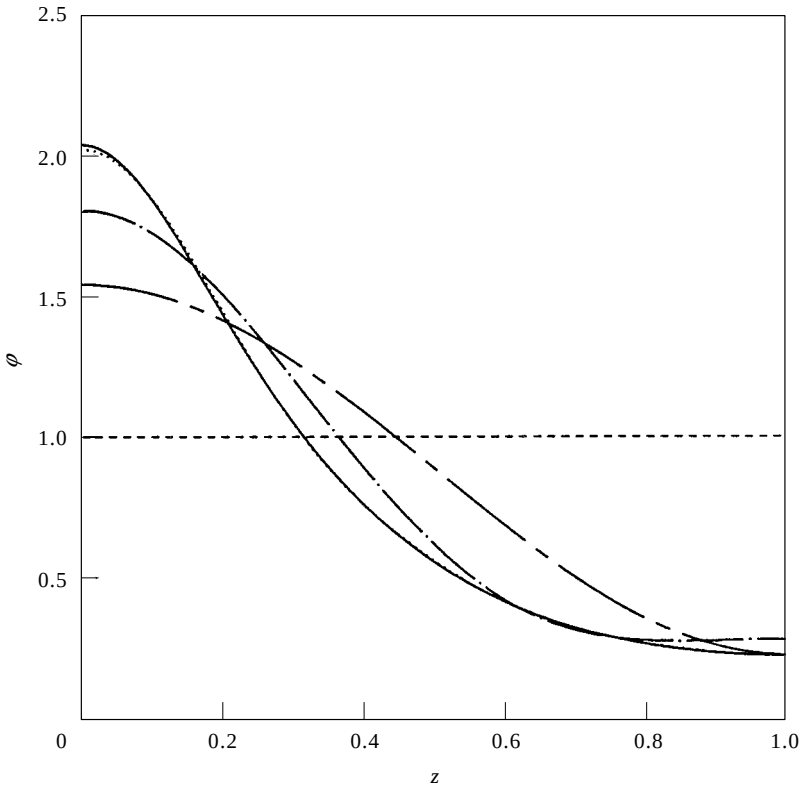

Figure 2. Longitudinal profiles of the acoustic pressure of the pure first tangential mode (1T-0L) for various numbers of trial functions with $n = 0$ corresponding to the Helmholtz eigenfunction. ——, $n = 10$; · · · ·, $n = 6$; — · — · , $n = 3$; — — — —, $n = 2$; – – – –, $n = 0$ or 1.

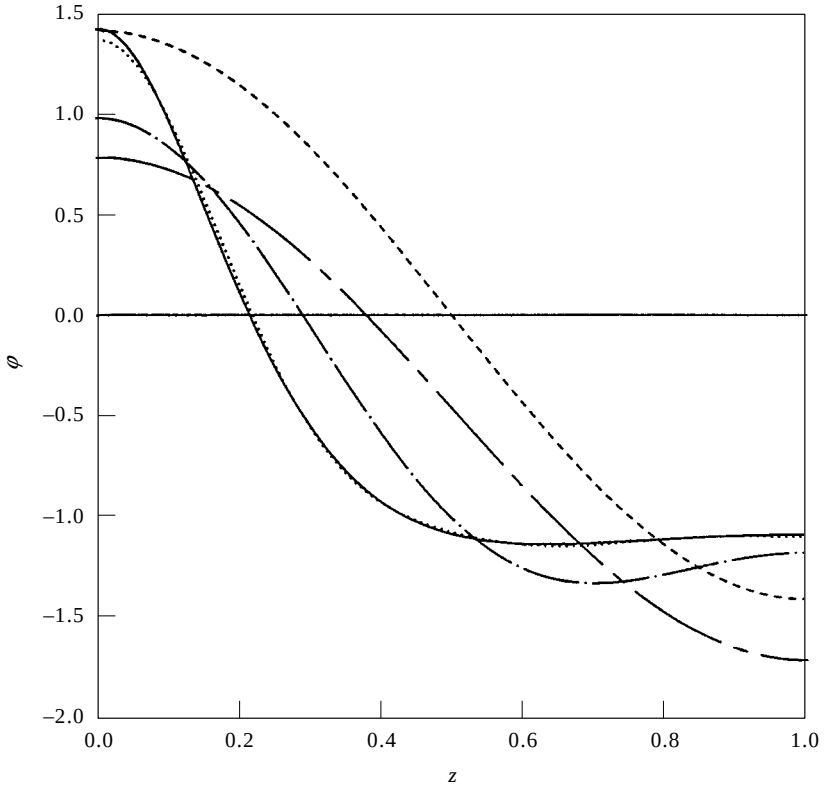

Figure 3. Longitudinal profiles of the acoustic pressure of the combined mode of the first tangential and the first longitudinal (1T-1L) for various numbers of trial functions with $n = 0$ corresponding to the Helmholtz eigenfunction. ——, $n = 10$; · · · ·, $n = 6$; — · — · —, $n = 3$; — – —, $n = 2$; – – – –, $n = 0$.

integrand $\rho_s^{-1} \nabla\psi \cdot \nabla\psi$ throughout the integral domain. Therefore, *the acoustic pressure gradient $\nabla\psi$ will be larger in the high-density region*, and smaller in the low-density region. Such behavior can be observed in Figure 4, where a much steeper variation of the acoustic pressure can be found in the high-density region near the entrance of the combustion chamber. This type of acoustic-pressure profile was reported experimentally already in early work by Levine [29], in which the variation was so pronounced that the measured pressure signal at the entrance of the nozzle section showed negligible pressure fluctuations. The nodes of the acoustic modes are consequently shifted toward the high-density region as observed in acoustic ducts with axial temperature gradient [15]. For instance, considering the combined mode of the first tangential and the first longitudinal (1T-1L), the Helmholtz eigenfunction (uniform chamber) predicted the location of the node at the middle of the chamber length, i.e., $z = 0.5$, as seen from the dashed line of Figure 3. The solution which includes the variable density profile shows that the node is located at about $z = 0.25$, thereby predicting a significant shift of the node toward the injector side. Such nodal shifts are also observed in Figure 4 for the higher combined modes, 1T-2L and 1T-3L.

It may also be noted that the matrix L_{ij} is tridiagonal, a result which arises from the fact that the density profile in equation (37) contains only the first harmonic term. For this type of density profile, exchange of the kinetic acoustic energy occurs only to adjacent modes, which follows from the tridiagonality of the matrix L_{ij}. If an acoustic mode receives energy from the adjacent lower mode, it passes a portion of its acoustic energy to the

adjacent higher mode, thereby forming a kind of acoustic kinetic energy cascade. This type of energy exchange mechanism explains why the pure first tangential mode has the largest eigenvalue shift from the corresponding Helmholtz eigenvalue among the pure and combined first tangential modes. The mode 1T-0L is the lowest first tangential mode and only loses its acoustic kinetic energy to the higher modes. On the other hand, the combined first tangential modes are able to receive energy from the adjacent lower modes and pass it to the adjacent higher modes. Since the eigenvalue σ is the ratio of the acoustic kinetic energy to the acoustic potential energy, the eigenvalue reduction by the density variation will be largest for the mode 1T-0L. For the same reason, all of the pure transverse modes are expected to have very large reductions of the eigenvalues if a considerable longitudinal density variation exists. For the same density profile in equation (37), the additional results of the eigenvalues for higher transverse modes are shown in Table 1. The density correction for the pure transverse modes increases for higher transverse modes and can be larger than 50%. On the other hand, the combined modes all have almost the same percentage corrections.

As seen from Table 1, acoustic frequencies of distributed media are always smaller than those of uniform media. A simple alternative explanation of this phenomenon can be obtained by considering one-dimensional wave propagation in which an acoustic wave is traveling from $x = 0$ to $x = 1$. Let the sound speed of the medium be given by

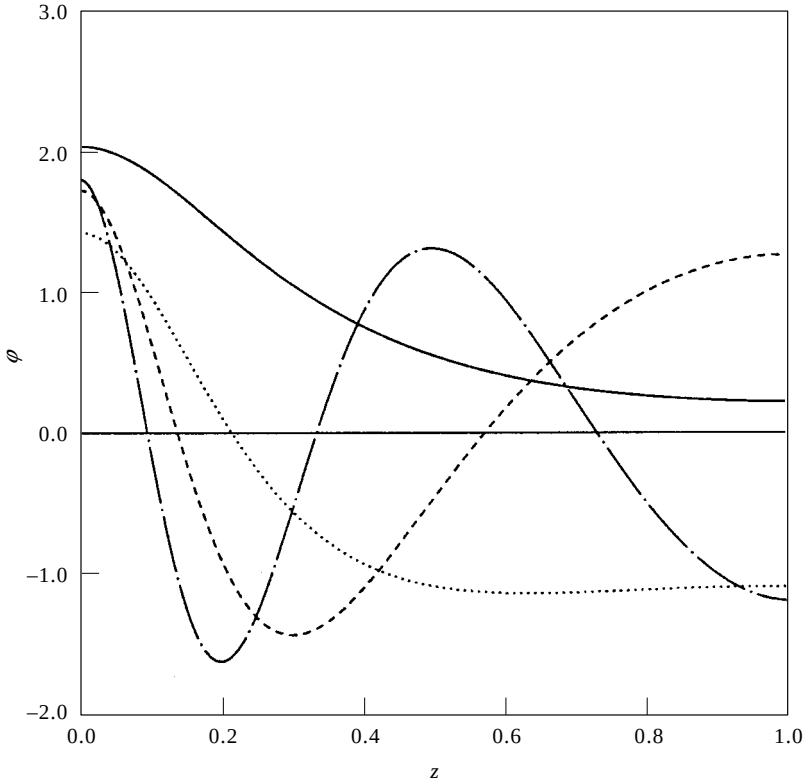

Figure 4. Longitudinal profiles of the acoustic pressure for the pure and combined first tangential modes: ——, 1T-0L; · · · ·, 1T-1L; – – – –, 1T-2L; — — — — —, 1T-3L.

$a = \bar{a}\{1 + \varepsilon f(x)\}$, where ε is a small parameter, and $\bar{a}$ is the averaged sound speed, so that $\int_0^1 f(x)\,\mathrm{d}x = 0$. The time required for the acoustic wave to complete a round trip is

$$\tau = 2\int_0^1 \frac{\mathrm{d}x}{\bar{a}\{1 + \varepsilon f(x)\}} \approx \frac{2}{\bar{a}}\left(1 + \varepsilon^2 \int_0^1 f^2\,\mathrm{d}x\right), \tag{41}$$

where terms of order higher than ε^2 are ignored. Since the acoustic frequency in this system is proportional to the number of round trips that the acoustic wave can make in a unit time, the acoustic frequency becomes

$$\omega = \frac{2\pi}{\tau} \approx \pi\bar{a}\left(1 - \varepsilon^2 \int_0^1 f^2\,\mathrm{d}x\right), \tag{42}$$

Here the integral $\int_0^1 f^2\,\mathrm{d}x$ is positive semi-definite and vanishes only if the medium is uniform. A uniform medium thus always has the fastest acoustic oscillation, and the acoustic frequency decreases with increasing non-uniformity of the medium.

4.4. APPROXIMATION BY PERTURBATION ANALYSIS

Parametric results for small degrees of non-homogeneity can be obtained by using a perturbation analysis. As an example, the density profile is assumed to be given by

$$\frac{1}{\rho_s} = 1 - \varepsilon \cos \pi z, \tag{43}$$

where ε is the small parameter of expansion. The matrices L_{ij} and M_{ij} are expanded in the form

$$L_{ij} = L_{ij}^{\{0\}} + \varepsilon L_{ij}^{\{1\}}, \qquad M_{ij} = M_{ij}^{\{0\}}. \tag{44}$$

Then the matrices L_{ij} and M_{ij} are found to be

$$L_{ij}^{\{0\}} = [k_{11}^2 + (i-1)^2\pi^2]\delta_{ij}, \qquad M_{ij}^{\{0\}} = \delta_{ij},$$

$$L_{ij}^{\{1\}} = \begin{cases} -k_{11}^2/\sqrt{2} & \text{if } ij = 2, \\ -[k_{11}^2 + (i-1)(j-1)\pi^2]/2 & \text{if } |i-j| = 1 \text{ and } ij \neq 2, \\ 0 & \text{otherwise.} \end{cases} \tag{45}$$

The eigenvalues and eigenvectors are sought in the form,

$$\sigma_r = \sigma_r^{\{0\}} + \varepsilon\sigma_r^{\{1\}} + \varepsilon^2\sigma_r^{\{2\}} + \cdots, \qquad c_{i,r} = c_{i,r}^{\{0\}} + \varepsilon c_{i,r}^{\{1\}} + \varepsilon_{i,r}^{\{2\}} + \cdots. \tag{46}$$

Substituting equations (44) through (46) into equation (32) and the orthonormality condition, the eigenvalue problem at each order is obtained as

$$[L_{ij}^{\{0\}} - \sigma_r^{\{0\}}\,\delta_{ij}]c_{j,r}^{\{0\}} = 0, \qquad \sum_i c_{i,r}^{\{0\}}\,c_{i,r}^{\{0\}} = 1,$$

$$[L_{ij}^{\{0\}} - \sigma_r^{\{0\}}\,\delta_{ij}]c_{j,r}^{\{1\}} = \sigma_r^{\{1\}}\,c_{i,r}^{\{0\}} - L_{ij}^{\{1\}}\,c_{j,r}^{\{0\}}, \qquad \sum_i c_{i,r}^{\{1\}}\,c_{i,r}^{\{0\}} = 0,$$

$$[L_{ij}^{\{0\}} - \sigma_r^{\{0\}}\,\delta_{ij}]c_{j,r}^{\{2\}} = \sigma_r^{\{2\}}\,c_{i,r}^{\{0\}} + \sigma_r^{\{1\}}\,c_{i,r}^{\{1\}} - L_{ij}^{\{1\}}\,c_{j,r}^{\{1\}}, \qquad \sum_i [2c_{i,r}^{\{2\}}\,c_{i,r}^{\{0\}} + c_{i,r}^{\{1\}}\,c_{i,r}^{\{1\}}] = 0. \tag{47}$$

At the leading order, the eigenvalue and eigenvector are identical to those of the Helmholtz equation, the r-th eigenpair being given by

$$\sigma_r^{\{0\}} = k_{11}^2 + (r-1)^2\pi^2, \qquad c_{i,r}^{\{0\}} = \begin{cases} 1 & \text{if } i = r, \\ 0 & \text{if } i \neq r. \end{cases} \tag{48}$$

For the first-order correction of the 1T-0L mode, consideration of the terms in the first row ($i = 1$, $r = 1$) in the second of equation (47),

$$[L_{1j}^{\{0\}} - \sigma_1^{\{0\}}\,\delta_{1j}]c_{j,1}^{\{1\}} = 0, \qquad \sigma_1^{\{1\}}\,c_{1,1}^{\{0\}} = \sigma_1^{\{1\}}, \qquad L_{1j}^{\{1\}}\,c_{j,1}^{\{0\}} = 0,$$

shows that the first-order correction for the eigenvalue, $\sigma_1^{\{1\}}$, is zero. Comparison of the second row yields

$$c_{2,1}^{\{1\}} = \frac{k_{11}^2}{\sqrt{2}\pi^2}, \tag{49}$$

while the other components of the eigenvector are found to be zero. As discussed in the previous section, the first non-trivial correction for the eigenvalue is of order ε^2, while the non-trivial correction for the eigenvector is of order ε. The second-order correction can be obtained in a similar way to be

$$\sigma_1^{\{2\}} = -\frac{k_{11}^4}{2\pi^2}, \quad c_{i,1}^{\{2\}} = \begin{cases} -k_{11}^4/4\pi^4 & \text{if } i = 1, \\ k_{11}^4\,[k_{11}^2 + 2\pi^2]/8\sqrt{2}\pi^4 & \text{if } i = 3, \\ 0 & \text{otherwise.} \end{cases} \tag{50}$$

With an accuracy up to order ε^3, the eigenvalue and eigenvector for the first tangential mode are then given by

$$\sigma_1 = k_{11}^2\left(1 - \varepsilon^2\frac{k_{11}^2}{2\pi^2} + \cdots\right), \quad c_{i,1} = \begin{pmatrix} 1 - \varepsilon^2 k_{11}^4/4\pi^4 \\ \varepsilon k_{11}^2/\sqrt{2}\pi^2 \\ \varepsilon^2 k_{11}^2\,[k_{11}^2 + 2\pi^2]/8\sqrt{2}\pi^4 \\ \mathcal{O}(\varepsilon^3) \\ \vdots \end{pmatrix}. \tag{51}$$

Comparisons of these three-term perturbation solutions with the numerical solutions are made here for $\varepsilon = 1/3(\rho_{max}/\rho_{min} = 2)$ and $\varepsilon = 3/4(\rho_{max}/\rho_{min} = 7)$. The axial distributions of the acoustic pressure amplitudes are shown in Figure 5. For $\varepsilon = 1/3$, an excellent agreement between the perturbation solution and numerical solution is found for the entire axial co-ordinate. On the other hand, the agreement for $\varepsilon = 3/4$ is seen to be much worse, although the feature that the acoustic amplitude of head pressure is higher than that of tail pressure is properly captured in the perturbation analysis. Figure 6 shows comparison of the eigenvlaues and demonstrates excellent agreement for the entire range of ε. However, the good agreement here for ε near unity is fortuitous in that it does not extend to higher modes.

The same method can be applied to analyze the effect of the variation in the adiabatic compressibility by assuming that the profiles of the properties are given by

$$\kappa_s = 1 + \varepsilon\cos\pi z, \qquad \frac{1}{\rho_s} = 1. \tag{52}$$

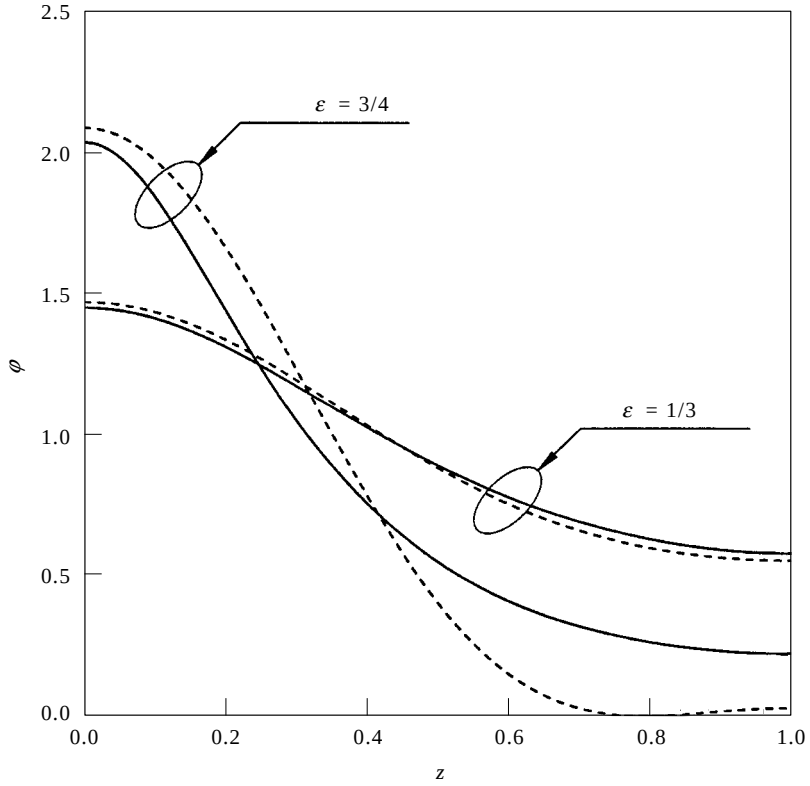

Figure 5. Comparison of the acoustic pressure profiles obtained by the numerical solution and three-term perturbation solution for the first tangential mode (1T-0L) with $\varepsilon = 1/3$ and 3/4. ——, Numerical; – – – –, perturbation.

With details omitted for brevity, the eigenvalue and eigenvector for the first tangential mode are found with an accuracy of up to order ε^3 to be

$$\sigma_1 = k_{11}^2\left(1 - \varepsilon^2\frac{k_{11}^2}{2\pi^2} + \cdots\right), \quad c_{i,1} = \begin{pmatrix} 1 - \varepsilon^2 k_{11}^4/4\pi^4 \\ \varepsilon k_{11}^2/\sqrt{2}\pi^2 \\ \varepsilon^2 k_{11}^4/8\sqrt{2}\pi^4 \\ \vdots \end{pmatrix}. \tag{53}$$

Here the second-order correction for the eigenvalue from variation of the adiabatic compressibility is found to be identical to that from variation of the density. The first-order correction for the eigenvector shows that *the acoustic pressure amplitude is higher in the region of high compressibility*. The behavior can be understood by considering the minimizing action of the functional given in equation (23). When the profile of κ_s is not uniform, minimization of the functional can be achieved by distributing the integrand of the denominator, i.e., $\kappa_s \psi^2$, more unevenly. Therefore, the acoustic pressure amplitude tends to be higher in the region where κ_s is larger.

The same perturbation method can be applicable to higher modes. However, the effectiveness of the perturbation method deteriorates very rapidly for higher modes. The correction terms become larger, and more terms in the expansion are needed. However,

for the lower modes, such as the first tangential mode, the perturbation method is found to be a satisfactory approximation method even for realistically large property variations. This is especially noteworthy because the lower modes are of greater practical importance for combustion instabilities.

4.5. IMPLICATIONS OF THE RESULTS FOR COMBUSTION INSTABILITIES

In liquid-propellant rocket engines, the excited acoustic modes usually begin with the smallest eigenvalue. Most of the modes observed in engines with moderate chamber aspect ratios are pure tangential modes, since their eigenvalues are smaller than those of combined modes. For these pure tangential modes, variation of the axial density profile can significantly influence combustion instability. The present analysis for pure tangential modes shows that the acoustic pressure and velocity amplitudes near the injectors are much larger than those near the nozzle. In order to investigate the effect of the longitudinal mean-density variation on acoustic amplification, we may write the linear amplification rate α as [3, 23]

$$\alpha = \int_{\mathscr{V}} q_1 \, \wp_1 \, \mathrm{d}V = \int_{\mathscr{V}} \mathbf{R}_p \, \wp_1^2 \, \mathrm{d}V + \int_{\mathscr{V}} \mathbf{R}_v \cdot \mathbf{v}_1 \, \wp_1 \, \mathrm{d}V, \tag{54}$$

where the leading-order fluctuation of the volumetric heat release rate q_1 in equation (11) is decomposed into contributions from the pressure response R_p and from the velocity

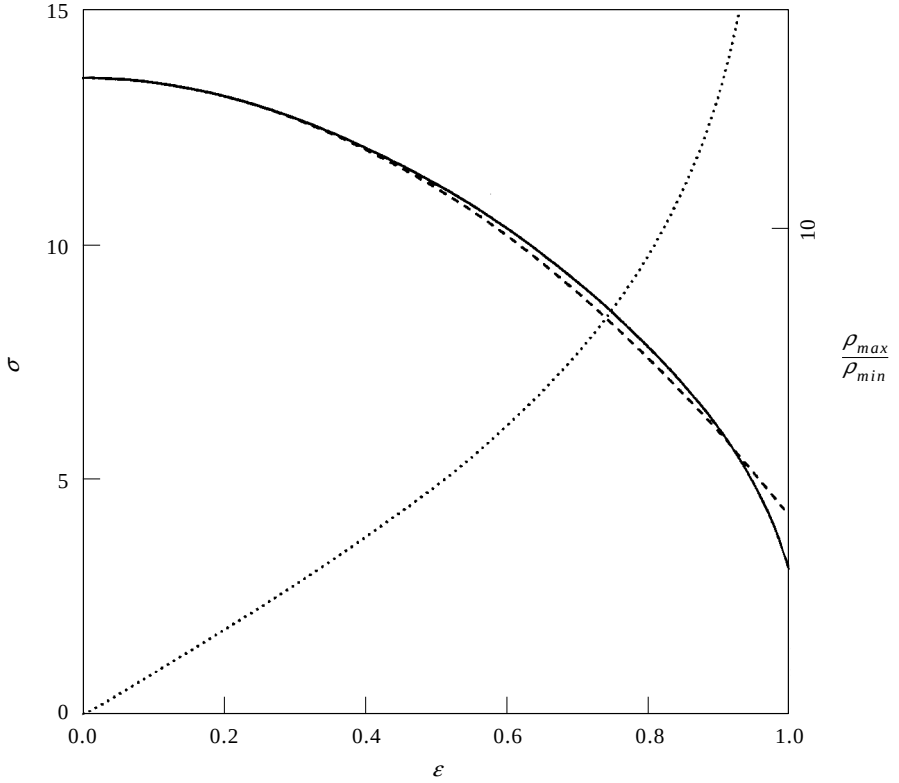

Figure 6. Comparison of the eigenvalues obtained by the numerical solution and three-term perturbation solution for the first tangential mode (1T-0L). ——, σ: numerical; – – – –, σ: perturbation; · · · · ·, ρ_{max}/ρ_{min}.

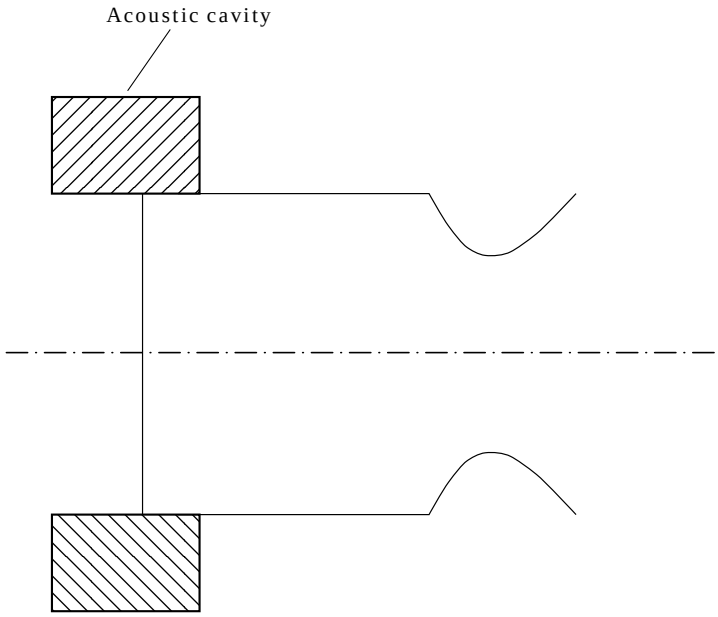

Figure 7. Schematic diagram of liquid propellant rocket engine with acoustic cavity around circular side wall.

response R_v as $q_1 = R_p \wp_1 + \mathbf{R}_v \cdot \mathbf{v}_1$. If spatial distributions of R_p and $\mathbf{R}_v$ can be obtained, then the present results can be used to evaluate the integrals in equation (54) and thereby to determine the amplification rate. In general, both the acoustic amplitude and the values of R_p and $\mathbf{R}_v$ tend to be greatest upstream for pure tangential modes. Therefore, it may be concluded from the present study that contributions to their linear growth rates come mainly from the region near the injector.

The more accurate acoustic pressure profiles provide useful information in determining the lengths of baffles or acoustic liners needed to suppress instability. Since the linear damping rate increases with increasing acoustic amplitude, it is more effective to install the damping devices where the acoustic pressure and velocity variations are larger. The present study suggests optimum lengths of about 25% of the chamber length. Another strategy for achieving a damping effect is to try to shift the region of high acoustic pressure out of the combustion zone by adding a high-density cavity to the chamber, perhaps by placing an acoustic cavity around the corner of the injector assembly at the side wall, as shown in Figure 7. Cooling of the cavity to maintain higher density could also be helpful. These conclusions follow from the general ideas developed here concerning density effects, ideas that complement those based on liner admittance, for example.

5. CONCLUDING REMARKS

The present analysis deals with effects of spatial variations of the density and adiabatic compressibility (or sound speed) on the acoustic eigenmodes in combustion chambers. The variations of those properties arise from a variety of sources such as progress of the combustion and evaporation of liquid fuels. The variational method employed here states that an eigenvalue, proportional to the square of an acoustic frequency, is the ratio of the kinetic acoustic energy to the static acoustic energy and that the associated eigenfunction

is the minimizing function of this ratio. Application to longitudinal property variations showed appreciable effects on frequencies and modes shapes.

Although our interest in the present analysis was aroused by questions about acoustics in liquid-propellant rocket engines, the same method can be applied to other combustion devices, such as pulse combustors and waste incinerators, in which acoustic pressure oscillation plays an essential role to enhance the performance. In these devices, the acoustic characteristics can be tailored by distributing properly the heat source or modifying boundary conditions, and these effects can be analyzed by the variational method demonstrated in here. In view of recent developments in generation of admissible test functions for complicated configurations [30], the variational method is also applicable to addressing effects of the complicated geometry that may arise from baffles, supersonic nozzles, or non-uniform regression of solid fuels in solid-propellant or hybrid rocket engines.

The experimental results of density-profile and acoustic-profile measurements, near the bifurcation condition of acoustic instabilities of rocket engines, scarcely exist because acoustic instabilities of rocket engines usually result in severe damages of the engines in a very short time. In particular, density-profile measurement is further complicated by the nature of two-phase flow in liquid-propellant rockets. In order to obtain reliable measurements of the acoustic eigenmodes in rocket engines, it might be helpful to use a relatively low-energy rocket engines, such as small scale gaseous rocket engines. In this type of rocket engines, a scalar measurement, such as temperature measurement, may be able to yield the profiles of complete scalar-field variables by utilizing the definition of the mixture fraction. Therefore, the analytic results of linear and non-linear stability analyses can be more easily compared with the experimental results.

ACKNOWLEDGMENTS

The authors would like to thank Ben Zinn and Robert Jensen for bringing several references to our attention. This research has been supported by the US Air Force Office of Scientific Research through AFOSR Grant No. F49620-97-1-0098.

REFERENCES

1. L. Crocco and S. I. Cheng 1956 *Theory of Combustion Instability in Liquid Propellant Rocket Motors*. London: Butterworths Scientific Publications.
2. D. J. Harrje and F. H. Reardon (editors) 1972 *Liquid Propellant Rocket Instability*. NASA SP-194.
3. F. E. C. Culick and V. Yang 1995 *Progress in Astronautics and Aeronautics* **169**, 3–38. Overview of combustion instabilities in liquid-propellant rocket engines.
4. B. T. Zinn 1968 *AIAA Journal* **6**, 1966–1972. A theoretical study of nonlinear combustion instability in liquid-propellant rocket engines.
5. B. T. Zinn and E. A. Powell 1970 *Thirteenth Symposium* (*International*) *on Combustion*, 491–503. Nonlinear combustion instability in liquid-propellant rocket engines.
6. F. E. C. Culick 1971 *Combustion Science and Technology* **3**, 1–16. Nonlinear growth and limiting amplitude of acoustic oscillations in combustion chambers.
7. F. E. C. Culick 1994 *AIAA Journal* **32**, 146–169. Some recent results for nonlinear acoustics in combustion chambers.
8. A. Kapur, A. Cummings and P. Mungur 1972 *Journal of Sound and Vibration* **25**, 129–138. Sound propagation in a combustion can with axial temperature and density gradients.
9. A. Cummings 1977 *Journal of Sound and Vibration* **51**, 55–67. Ducts with axial temperature gradients: an approximation solution for sound transmission and generation.

10. M. G. Prasad and M. J. Crocker 1981 *Journal of the Acoustical Society of America* **69**, 916–921. Evaluation of a four parameters for a straight pipe with a mean flow and a linear temperature gradient.
11. W. H. Clark 1982 *Journal of Spacecraft and Rockets* **19**, 47–53. Experimental investigation of pressure oscillations in a side dump ramjet combustor.
12. M. El-Raheb and P. Wagner 1983 *Journal of the Acoustical Society of America* **74**, 1583–1596. Acoustic propagation in resonant axisymmetric cavities enclosing an inhomogeneous medium. Part I: hollow cavity.
13. M. L. Munjal and M. G. Prasad 1986 *Journal of the Acoustical Society of America* **80**, 1501–1506. On plane-wave propagation in a uniform pipe in the presence of a mean flow and temperature gradient.
14. K. S. Peat 1988 *Journal of Sound and Vibration* **123**, 43–53. The transfer matrix of a uniform duct with a linear temperature gradient.
15. R. I. Sujith, G. A. Waldherr and B. T. Zinn 1994 *AIAA Paper No*. 94-0359. Exact solution for one-dimensional acoustic fields in ducts with axial temperature gradient.
16. L. Meirovitch 1980 *Dynamics and Control of Structure*. New York: Wiley.
17. A. M. Laverdant, T. Poinsot and S. M. Candel 1986 *Journal of Propulsion and Power* **2**, 311–316. Mean temperature field effect on the acoustic mode structure in dump combustors.
18. T. A. Coultas 1972 *Liquid Propellant Rocket Instability NASA SP*-194. Combustion instability.
19. B. J. Matkowsky 1970 *SIAM Journal on Applied Mathematics* **18**, 872–883. Nonlinear dynamic stability: a formal theory.
20. S. B. Margolis 1993 *Journal of Fluid Mechanics* **253**, 67–84. Nonlinear stability of combustion-driven acoustic oscillations in resonance tubes.
21. P. Clavin, J. S. Kim and F. A. Williams 1994 *Combustion Science and Technology* **96**, 61–84. Turbulence-induced noise effects on high-frequency combustion instabilities.
22. F. A. Williams 1985 *Combustion Theory*. Menlo Park: Addison-Wesley.
23. J. S. Kim 1995 *Progress in Astronautics and Aeronautics* **169**, 431–454. Effects of turbulence on linear acoustic instability: spatial inhomogeneity.
24. P. M. Morse and K. U. Ingard 1968 *Theoretical Acoustics*. Princeton, NJ: Princeton University Press. See pp. 407–414.
25. L. D. Landau and E. M. Lifshitz 1987 *Fluid Mechanics*. New York: Pergamon Press. See pp. 292–294.
26. P. M. Morse and H. Feshbach 1953 *Methods of Theoretical Physics*. New York: McGraw-Hill.
27. I. M. Gelfand and S. V. Fomin 1963 *Calculus of Variations*. Englewood Cliffs, NJ: Prentice-Hall.
28. C. M. Bender and S. A. Orszag 1978 *Advanced Mathematical Methods for Scientists and Engineers*. New York: McGraw-Hill.
29. R. S. Levine 1965 *Tenth Symposium* (*International*) *on Combustion*, 1083–1099. Experimental status of high frequency liquid rocket combustion instability.
30. V. Yang, M. W. Yoon and J. M. Wicker 1993 *AIAA Paper No*. 93-0233. Nonlinear pressure oscillations in baffled combustion chambers.

APPENDIX A: FLUID PROPERTIES IN MULTIPHASE MIXTURES

Consider a multiphase system consisting of a number of liquid phases dispersed in an ideal-gas mixture, and let $\tilde{\rho}_{ji}$ denote the mass of chemical species i in phase j per unit volume of phase j and α_j the volume fraction of phase j. Generally $j = g, f, o$ denotes gas, fuel and oxidizer streams, respectively, although $j = g$ only, with $\alpha_g = 1$, when the flow is at totally supercritical conditions. With N chemical species in the system, the density of phase j, denoted by $\tilde{\rho}_j$, and the total density, denoted by $\tilde{\rho}$, are

$$\tilde{\rho}_j = \sum_{i=1}^{N} \tilde{\rho}_{ji}, \qquad \tilde{\rho} = \sum_j \alpha_j \tilde{\rho}_j. \tag{A1}$$

From the above definitions, we are able to define the mass fractions, namely

$$Y_j = \frac{\alpha_j \tilde{\rho}_j}{\tilde{\rho}}, \qquad Y_{ji} = \frac{\alpha_j \tilde{\rho}_{ji}}{\tilde{\rho}}, \qquad \text{with} \quad \sum_j Y_j = 1, \qquad \sum_i Y_{ji} = Y_j, \tag{A2}$$

where Y_j is the mass fraction of phase j, and Y_{ji} is that of species i in phase j.

To consider the overall frozen sound speed, we first write the overall density as

$$\tilde{\rho} = \frac{\tilde{m}}{\tilde{V}} = \frac{\sum_j \tilde{m}_j}{\sum_j \tilde{V}_j}, \tag{A3}$$

where $\tilde{m}_j$ is the mass of phase j in a small control volume $\tilde{V}$ and $\tilde{V}_j$ is the volume of phase j in that control volume. In the frozen sound speed, the differential operator acts only on the $\tilde{V}_j$'s, so that

$$\frac{1}{\tilde{a}_f^2} = \left(\frac{\partial \tilde{\rho}}{\partial \tilde{p}}\right)_{\tilde{s}, Y_{ji}} = -\sum_j \frac{\tilde{m}}{\tilde{V}^2} \left(\frac{\partial \tilde{V}_j}{\partial \tilde{p}}\right)_{\tilde{s}, Y_{ji}}, \tag{A4}$$

where $\tilde{s}$ is the total entropy per unit mass. From the definition of the frozen sound speed of phase

$$\frac{1}{\tilde{a}_{f,j}^2} = -\frac{\tilde{m}_j}{\tilde{V}_j^2} \left(\frac{\partial \tilde{V}_j}{\partial \tilde{p}}\right)_{\tilde{s}, Y_{ji}}, \tag{A5}$$

the overall frozen sound is expressed as

$$\frac{1}{\tilde{a}_f^2} = \sum_j \frac{\alpha_j^2}{Y_j} \frac{1}{\tilde{a}_{f,j}^2}. \tag{A6}$$

In liquid-propellant rocket motors, the volume fraction of each liquid phase is usually small, and the sound speed is higher in the liquid phase than in the gas phase, so that the overall sound speed can be approximated as being determined by that of the gas phase only. Since the gas phase is assumed to be an ideal-gas mixture, the overall frozen sound speed is expressed as

$$\tilde{a}_f^2 \approx \frac{Y_g \tilde{a}_{f,g}^2}{\alpha_g^2} \approx \frac{Y_g \gamma_g \tilde{R} \tilde{T}_g}{\alpha_g^2}, \tag{A7}$$

where $\tilde{T}_g$ is the gas temperature, γ is the ratio of the specific heat at constant pressure to that at constant volume, and $\tilde{R}$ is the gas constant per unit mass for the gas phase.

The adiabatic compressibility $\tilde{\kappa}_f$ in equation (2) is then correspondingly approximated as

$$\tilde{\kappa}_f = \frac{1}{\tilde{\rho} \tilde{a}_f^2} \approx \frac{Y_g}{\alpha_g} \frac{1}{\tilde{\rho}_g \tilde{a}_f^2} \approx \frac{\alpha_g}{\gamma_g \tilde{p}_g}, \tag{A8}$$

where $\tilde{p}_g$ is the pressure in the gas phase, and use is made of equations (A2) and (A7) for the second and third approximations, respectively. Since the pressure in the gas phase is

almost constant throughout the rocket chamber, the adiabatic compressibility is proportional mainly to the volume fraction of the gas phase.

APPENDIX B: NOMENCLATURE

D	chamber diameter
$\mathbf{F}$	momentum source
L	rocket-chamber length
$\mathscr{L}$	differential operator defined in equation (20)
L_{ij}	matrix form of the operator $\mathscr{L}$ as defined in equation (31)
M	Mach number as defined in equation (5)
$\mathscr{M}$	weighting function defined in equation (20)
M_{ij}	matrix form of the weighting function $\mathscr{M}$ as defined in equation (31)
Q	energy source
R	Rayleigh quotient as defined in equations (27) or (30)
V	total volume of integration domain
$\mathscr{V}$	integration domain illustrated in Figure 1
a	sound speed
e	acoustic energy as defined in equation (39)
$\mathbf{f}$	acoustic part of momentum source as shown in equation (11)
k	wave number
m	area-averaged axial mass flux
$\mathbf{n}$	unit outward normal vector at the boundary
p	pressure
$\wp$	acoustic pressure as expanded in equation (11)
q	acoustic part of energy source as shown in equation (11)
r	radial co-ordinate
t	time co-ordinate
$\mathbf{u}$	velocity vector
$\mathbf{v}$	acoustic velocity vector as expanded in equation (11)
$\mathbf{x}$	spatial co-ordinate vector
z	longitudinal co-ordinate

Greek symbols

α	linear amplification rate
ε	small expansion parameter for acoustic amplitude
ϵ	small expansion parameter for sound speed or density variation
θ	azimuthal co-ordinate
κ	line alignment adiabatic compressibility
λ	non-dimensional acoustic frequency as defined in equation (16)
ρ	density
ϱ	acoustic part of density as shown in equation (11)
$\sigma \equiv \lambda^2$	eigenvalue of the modified Helmholtz equation
ψ	amplitude of the acoustic pressure oscillation
ω	acoustic frequency

Superscripts

$\tilde{()}$	dimensional quantities
$()^{(n)}$	n-dimensional subspace of admissible functions
$()^{\{0\}}, \ldots$	expansion orders associated with ε

Subscripts

$()_0$	volume-averaged reference state
$()_1, \ldots$	expansion orders for the acoustic field
$()_f$	frozen state
$()_s$	steady state